Multiple-scan voltammetry and OCP: archaeometric tools for dating archaeological bronzes

Antonio Doménech-Carbó*[a], Marianne Mödlinger[b], María Teresa Doménech-Carbó[c]

[a] Departament de Química Analítica. Universitat de València. Dr. Moliner, 50, 46100 Burjassot (València) Spain.
[b] Dipartimento di Chimica e Chimica Industriale, Universitá degli Studi di Genova, Via Dodecaneso 31, 16126 Genova, Italy.
[c] Institut de Restauració del Patrimoni, Universitat Politècnica de València, Camí de Vera 14, 46022, València Spain.

* Corresponding author: e-mail: antonio.domenech@uv.es

Abstract

The application of a multiple-scan strategy to nanosamples taken from 18 cross-sections of Bronze Age arms and armour, as well as two Roman coins using two solid-state electrochemical techniques, the voltammetry of immobilized microparticles (VIMP) and open circuit potential measurements (OCP) is described. The voltammetric responses in contact with aqueous acetate buffer can be attributed to the reduction of cuprite with variable degree of compaction and crystallinity revealing significant differences in the gradient of such properties with depth. Such differences are also revealed by "dry" OCP measurements connecting points in the cross section near and saeparated from the corrosion layer. The voltammetric study of the metallographic samples of the bronze objects shows correlation with the age of the objects, respectively the period of their deposition. We discuss also (potential) influence of different factors on the VIMP and OCP measurements, such as deposition context (soil, water), chemical composition of the copper alloys, and microstructural features (as-cast, annealed, work-hardened), and how to overcome these issues.

Keywords: Voltammetry of immobilized particles; OCP; e Age; dating archaeological bronzes; corrosion studies.

1. Introduction

The fundamental copper and copper alloy working technologies developed in prehistory are well known from standard metallurgical analysis techniques [1]. These techniques are often destructive and cannot be used on one-of-a-kind or otherwise valuable artefacts. Acquiring information on archaeological metal and technology is therefore problematic since information is required not only on surface examinations but their chemical composition and microstructure, which, in most instances, requires the use of invasive analytical techniques [2,3]. Due to limitations imposed by the desire to protect unique and otherwise valuable cultural objects from harm [4-6], extensive research on anti-corrosion procedures [7-10] accompanies the development of minimally invasive techniques have been developed capable of yielding otherwise inaccessible archaeological information [].

Regarding noninvasive techniques, the voltammetry of immobilized particles (VIMP), a solid-state electrochemistry technique developed by Scholz et al. [19-21], has emerged as an interesting archaeoanalytical tool since it requires small samples at the sub-microgram level from the corrosion patina of the objects. This technique is highly sensitive and arguably non-destructive [22-25]. Sampling for VIMP consists of the abrasive transference of a fraction of a solid to an inert electrode, typically paraffin-impregnated graphite. The sample-modified electrode is then immersed in a suitable electrolyte where the solid is sparingly soluble, and the voltammetric response is recorded. This method has been widely applied to the study of metal objects where sampling is made merely by pressing a graphite pencil onto the artifact's surface, resulting in a few nanograms of the patina being transferred to the graphite surface. Based on the above sampling methodology, VIMP has been used to discriminate the provenances, manufacturing techniques [26-30], characterizing artificial patinas [31], and dating [32] of copper alloy objects based on the analysis of cathodic signals associated with the reduction of (mainly) cuprite and tenorite components of patina.

In this context, we have recently developed a novel technique, "dry" open-circuit potential (OCP) measurements, applying it to the study of archaeological iron objects [33]. This technique expands the methodologies applied for corrosion evaluation in reinforcements embedded in concrete [34-36] and consists of the record of the potential difference between two points of the archaeological artifact. One point corresponds to the conducting regions where the metallic core is covered by a layer of conducting oxides. By obvious reasons of minimal object deterioration, the wet reference

electrode (typically Cu/CuSO₄) connected to the concrete surface by a wet sponge or paper) was replaced by entirely dry connections.

In this paper, we present the novel application of the VIMP and OCP techniques to a series of cross-section metallographic samples from a set of Bronze Age objects embedded in epoxy resin previously studied by conventional metallographic and chemometallographic techniques [37-41]. The re-use of previously studied samples without new sampling implies an optimization of the existing analytical resources with null additional deterioration of the archaeological object. A multiple-scan strategy using square wave voltammetry (SWV) has been adopted for VIMP measurements. This methodology was previously adopted for the analysis of several 18th to 20th century coins with satisfactory results [42]. The samples are an interesting assemblage of objects that include high-status items, representing the peak of metallurgical technology during the European Bronze Age.

2. Experimental

2.1. Samples

A set of 18 bronze cross-sections from Bronze Age swords and sheet metal work, and two cross-sections from Roman coins from different archaeological sites in Central and Eastern Europe (Austria, Slovenia, Ukraine, Czech Republic, Romania, Croatia, and Bosnia-Herzegovina), were studied. All were bright yellow-orange in color, which is typical of freshly cut copper objects. Figure 1 shows a selection of images from some of the original studied archaeological objects, including a a fragment of a (reconstructed, see drawing) decorated cap helmet from Veliko Nabrđe, Croatia, a sword from Viljĥovicja (Vulchovica), Ukraine,and a knob from a helmet from Grepci, Bosnia-Herzegovina. The reconstructed images of the original artifacts are accompanied by reconstructions of the same. Data for the samples are summarized in Table 1. All of the tested samples show a similar chemical composition of 86-92 wt.% Cu, 8-13 wt.% Sn, and a maximum of 1.6 wt.% Pb. Through metallographic analysis, the samples were grouped as follows:

- Samples **1**-**6:** cast; annealed/cold deformation at the edge; cold deformation as final working step
- Samples **7**, **8:** cast, final cold deformation at the edge
- Samples **9**-**18:** sheet metal; cast; annealed/cold deformation; cold deformation as final working step
- Samples **19**, **20:** cast Roman coins; one of them was hallmarked

2.2. Electrochemical instrumentation and methods

Sampling for the VIMP measurements was performed by pressing the edge of a graphite bar (Alpino Maxim, HB type pencil) of 2 mm diameter onto the cross-section's surface. Three - five measurements were performed on each cross-section depending on its surface area. The lower end of the sample-modified graphite electrode was then immersed into the electrolyte to carry out the voltammetric measurements. The experiments were performed using a CH I660c potentiostat (Cambria Scientific, Llwynhendy, Llanelli UK) coupled with a three-electrode cell platinum auxiliary electrode and an Ag/AgCl (3M NaCl) reference electrode. De-aerated 0.25 M HAc/NaAc (Probus reagents) solution at pH 4.75 was used as a supporting electrolyte.

OCP measurements on cross sections were made in the university laboratories at 20 ºC and 70% RH using a CH 920c potentiostat connecting the reference and working electrode terminals through crocodile clamps to two graphite bars (Alpino CH type) of 2 mm diameter finished in conic sections of 0.5 mm diameter put in contact with the selected points of the bronze cross-sections. These points were selected, as schematized in Figure 2, i) having a separation of 0.5±0.1 cm, and ii) one being near the external patina in the subsurface region and one being in the metallic core. The electrodes were fixed pressing onto the cross-section surface with the aid of the arm of the SECM device associated to the potentiostat. Figure 2 depicts a scheme of the experimental arrangement used for OCP measurements. Control experiments were carried out with a cylindrical Faraday cage in order to test the possible influence of external electrical sources, with no signidficant differences between them, in agreement with previous results [42].

3. Results and discussion

3.1. VIMP measurements

Figure 3 depicts the multiple-scan SWV's of samples a) **2**, b) **4**, c) **7,** and d) **10** attached to graphite electrode in contact with 0.25 M HAc/NaAc aqueous solution at pH 4.75. Upon scanning the potential from 0.45 V vs. Ag/AgCl in the negative direction, a main cathodic peak appears at −0.10 V vs. Ag/AgCl (C_1), often accompanied by minor peak potentials or shoulders at ca. 0.05 V. In successive cathodic scans (N scans, from 1st to 6th), the intensity of the peak ($I_p(N)$) decreases. To interpret a sample's voltammetry, the analytical process requires removing a set of plates 1-5 μm-sized from the metal's patina, typically amounting to ca. 2 nanograms [42]. In the case of the

4

studied cross-sections, the main component is cuprite with a variable degree of compaction and crystallinity, coming from the defective cuprite forming the primary, passive patina over the copper (or bronze) metal [7, 43-45]. The following reaction describes the electrochemical process:

$$Cu_2O \text{ (solid)} + 2H^+ \text{ (aq)} + 2e^- \rightarrow Cu \text{ (solid)} + H_2O \quad (1)$$
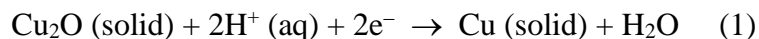
According to our previous theoretical models [42], the plates are delaminated in successive cathodic scans such that corresponding voltammetric parameters are representative of the composition of progressively deeper regions of the metal's patina. Then, the variation of the peak current (strictly, in SWV, the measured quantity is the difference peak current between the forward and backward currents measured at the beginning and end of each potential pulse) with the scan number (N) can be considered representative of the charge passed during the reduction of copper corrosion products, in turn, representative of the in-depth variation of the compaction and crystallinity of the metal's patina.

Figure 4a compares the variation with the scan number N of the peak current $I_p(N)$ in three spots on sample **3**. For the reasons already discussed [42], the accumulated peak current $Q_p(N)$, calculated as the sum of the peak currents in successive scans, was used. The corresponding values for sample **3** are depicted in Figure 4b. Such data can be approximated by polynomial or logarithmic functions taking N as a continuous variable, thus defining different functional profiles.

In this scenario, the values of $Q_p(N)$ should represent the variation of the patina's properties with depth, $Q_p(1)$ ($= I_p(1)$) corresponding to the more outer region. In cuprite patinas, as can be expected for cross-sections of bronze objects, the value of the peak currents should be larger for less compact patinas such that the gradient in the accumulated peak current will be representative of the gradient of compactness in the patina. However, since the net amount of sample transferred onto the graphite electrode cannot be accurately controlled, the above quantities' values in replicate experiments cannot be directly compared. In principle, this problem can be solved using the ratio between peak currents. Ultimately, if successive voltammetric scans result in the delamination of the patina's laminas, the region of the primary patina will be attained. Ideally, and given the tendency curves in Figure 4b, this corresponds to the limiting value of $Q_p(N)$ when $N \rightarrow \infty$, $Q_p(\text{lim})$.

Accordingly, the $Q_p(1)/Q_p(6)$ or $Q_p(1)/Q_p(\text{lim})$ ratios can be considered representative of the gradient of compaction/crystallinity of the cuprite patina in the sample. Since we analysed "fresh"

cross-sections, the difference in such quantities will reflect the differences in the manufacturing techniques employed in the artifact's fabrication. Our data, however, reflect relatively large differences in the 1st scan voltammogram (see Figure 3) that can be attributed to sample handling (later deposited organic matter) and residuals from sputtering applied carbon to facilitate electron microscopic examination of the cross-sections. For these reasons, the $Q_p(2)/Q_p(6)$ ratio or $Q_p(2)/Q_p(\text{lim})$ ratios were tested.

To determine $Q_p(\text{lim})$, a suitable $Q_p(N)$ vs. $1/N$ representation was used. Figure 5 shows the corresponding graphs obtained from three voltammetric measurements in different spots on sample **3**. Experimental data can be satisfactorily fitted to 2nd order polynomial functions where N is a continuous variable with correlation coefficients generally larger than 0.999 (see Table 2), thus providing a satisfactory confidence level for the extrapolated values of $Q_p(\text{lim})$.

For our purposes, the relevant point to emphasize is that the average values of the $Q_p(1)/Q_p(6)$ or $Q_p(1)/Q_p(\text{lim})$ ratios is significantly different across different samples. According to our theoretical treatment of a repetitive voltammetry applied to 18th to 20th century coins [42], such differences are representative of the gradient of compaction/crystallinity of cuprite in the patina.

Figure 6 shows an idealized, linear variation of $Q_p(N)$ with depth (z) for two different samples. Here, the idealized variation of $Q_p(N)$ with depth for two different bronze patinas is represented, assuming, for simplicity, that the successive scans similarly delaminate both patinas and that the accumulated peak current varies linearly with the depth. If the compaction/crystallinity gradient is sharp (left side of Figure 6), the $Q_p(2)/Q_p(\text{lim})$ ratio is higher than if that gradient is smooth (right side in Figure 6).

3.2. OCP measurements

Figure 7a shows typical OCP vs. time curves recorded in our "dry" electrochemistry experiments for samples **4** and **8**. The measured potencial, V_{OCP}, shows a moderately noisy variation with time that can be fitted to a relatively fast exponential decay tending to a limiting value with a variation of few mV. This result can in principle be rationalized, as previously discussed [33], on the basis of the general description of the structure of corrosion layers in archaeological bronze artifacts [46] and the modeling of corrosion processes [47,48]. As previously noted, we can expect that there is a smooth gradient of crystallinity, porosity, compaction, etc. in the cuprite patina covering the metal in the cross-section. Then, the potential difference between two points of the cross-section will

result from the difference in the work function of the metal corrosion product. This will act as the driving force associated to some charge transport where the humidity layer covering the cross-section will act as the electrolyte.

Consistently, a charging curve associated to either the double-layer charging and the space charge charging of the semiconducting patina (cuprite is a n-type semiconductor) was recorded. The equation for the charging current can be expressed by an exponential equation of the form:

$$V_{OCP} = V_{inic} + (V_{lim} - V_{inic})(1 - e^{-kt}) \qquad (2)$$

In this equation k represents a rate constant and V_{inic}, V_{lim} the OCPs at time zero and at infinite time. Accordingly, plots of $\ln(V_{OCP} - V_{lim})$ vs. t should provide straight lines of slope $-k$. Figure 7b shows the corresponding representations for samples 2, 3, and 11. In all cases, a satisfactory linearity was obtained, the k values ranging between 0.17 and 0.25 s^{-1}.

This response can be modeled on the basis of the equivalent circuit schematized in Figure 7c. It will be assumed that there is a charging process driven by the a contact potential (ø) between two semiconducting regions of the cross-section. The electrical circuit is closed through the external voltmeter and the conducting (electrolytic) fine wet layer covering the surface of the cross-section. Then, the circuit external to the voltmeter can be modeled by a Randles-type circuit containing a resistance r associated to the electrolyte in series with a parallel association of a charge-transfer resistance R and a double layer capacitance C. Then, the following equations apply:

$$\phi = i(r + R_V) + \frac{q}{C} \qquad (3)$$

$$i = I + \frac{dq}{dt} \qquad (4)$$

$$IR = \frac{q}{C} \qquad (5)$$

Then:

$$\phi - \frac{q}{C}\left(1 + \frac{r + R_V}{R}\right) = (r + R_V)\frac{dq}{dt} \qquad (6)$$

7

$$\int_0^q \frac{(r + R_\text{V})dq}{\phi - \dfrac{q}{C}\left(1 + \dfrac{r + R_\text{V}}{R}\right)} = \int_0^t dt \qquad (7)$$

Then, the charge at a time t and the OCP at this time will be:

$$q = \frac{C\phi}{1 + \dfrac{r + R_\text{V}}{R}}\left\{1 - \exp\left[-\frac{t}{(r + R_\text{V})C}\left(1 + \frac{r + R_\text{V}}{R}\right)\right]\right\} \qquad (8)$$

$$V_\text{OCP} = \phi\left(\frac{R}{R + r + R_\text{V}}\right)\left\{\frac{R_\text{V}}{R} + \exp\left[-\frac{t(R + r + R_\text{V})}{(r + R_\text{V})RC}\right]\right\} \qquad (9)$$

This equation is equivalent to Eq. (2) taking as initial (time zero) and limiting (infinite time) potentials:

$$V_{init} = \frac{\phi(R + R_V)}{R + r + R_V} \qquad (10)$$

$$V_\text{lim} = \frac{\phi R_V}{R + r + R_V} \qquad (11)$$

This means that the OCP measurements are conditioned by the internal resistance of the voltmeter. Under our experimental conditions, one can expect that $R_\text{V} \gg R + r$ so that the initial and limiting potentials should be almost identical to the contact potential, which in turn has to be low because we are connecting two regions of the cross-section. Since the uncertainty in the measurement of V_lim is clearly lower than the uncertainty in the measurement of V_init, it is convenient to use the former quantity for testing the differences between different cross-sections (vide infra). In agreement with the previous considerations, the values of V_lim in cross-sections is typically of few milivolts. In contrast, V_lim values around 0.2 V were obtained when conducting regions are connected with metal corrosion layers [33]. For our purposes, the relevant point to emphasize is that V_lim values provide information on subtle differences between the charge transport properties of different regions of the studied cross-sections.

3.3. Implications for dating

In view of the existence of light although consistent differences in the values of the VIMP and OCP parameters determined for the different cross-sections, we attempted to establish possible

correlations with the geographical location of the archaeological sites/theor deposition context, manufacturing techniques (known from previous metallographic analysis [37-41]), and age. The plot of averaged $Q_p(2)/Q_p(\text{lim})$ vs. age for samples **1**-**8**, all cast, annealed, and cold deformed, is shown in Figure 8a. Here, one can see that this set of data suggests a variation of $Q_p(2)/Q_p(\text{lim})$ and the age of the object within the studied period. Although with relatively high dispersion, this variation can be fitted to a potential function or an exponential function without significant difference between them. In contrast, the representation of $Q_p(2)/Q_p(\text{lim})$ vs. age for samples **9**-**18**, all constituted by sheet metal and final cold deformation, does not reveal any significant tendency, as can be seen in Figure 8b. In this set, the Qp(2)/Qp(lim) dispersion was higher than in samples **1**-**8**.

Remarkably, OCP patameters displayed variations with the age entirely consistent with those observed for VIMP parameters. This is illustrated in Figure 9 wehere the limiting potential, Vlim is plotted vs. the object age for samples **1**-**8**.

Conjointly considered, these results suggest that voltammetric data recorded from cross-sections of Bronze Age archaeological bronze objects enables us to confirm the existence of different metallographic patterns. Accordingly, VIMP data are useful to detect differences in applied manufacturing techniques. In the case of cast bronze objects, which underwent annealing and cold deformation, the voltammetric data suggest a chronological sequence potentially suitable for dating purposes. However, it is pertinent that, as far as we have studied "fresh" metal cross-sections rather than original corrosion patinas, the time variation of the electrochemical parameters in Figures 8a and 9 can be attributed to variations in the compaction/crystallinity of the metal patina. These variations can be attributed to technological differences of the Bronze Age objects. Consequently, VIMP and OCP can detect technological choices made during the production of bronze objects and provide further information on the age of archaeological metal artefacts.

4. Conclusions

The VIMP and "dry" OCP methods were applied to the study of Bronze Age swords and various sheet metal object cross-sections previously studied by other techniques. Application of a multiple-scan strategy to nanosamples from the cross-sections permitted the recording of characteristic voltammetric features representative of the in-depth variation of the compaction and crystallinity of cuprite that formed the metal's patina. Consistent results were obtained with the OCP technique.

The recorded differences in the VIMP and OCP responses appear to vary monotonically with time for Bronze Age swords and Roman coins, making this a potential technique for dating similar artefacts. However, no chronological tendency was detected on samples from sheet metal artifacts, which underwent several cycles of annealing/cold deformation with final cold deformation.

Given the virtually non-destructive character of the applied solid-state electrochemical methods (only few nanograms of metal patina are needed for analyses), all these data can be considered illustrative of the capabilities of VIMP and "dry" OCP to yield archaeometric information. Further analyses of a wider set of prehistoric bronze objects are in preparation, especially in order to clarify the influence of find context, microstructure, and chemical composition of the object on the measurements, and to create a calibration reference database for future measurements.

References

[1] B.W. Roberts, C. Thornton, Eds. Archaeometallurgy in Global Perspective. Methods and Syntheses, Springer, berlin, 2014.

[2] G. Bertrand, E. Rocca, C. Savall, C. Rapin, J.-C. Labrune, P. Steinmetz, In-situ electrochemical atomic force microscopy studies of aqueous corrosion and inhibition of copper, J. Electroanal. Chem. 489 (2000) 38–45.

[3] A. Xu, C. Dong, X. Wei, X. Li, D.D. Macdonald, DFT and photoelectrochemical studies of point defects in passive films on copper, J. Electroanal. Chem. 834 (2019) 216–222.

[4] D.A. Scott, An examination of the patina and corrosion morphology of some Roman bronzes, J. Am. Ite. Cons. 33 (1994) 1–23.

[5] L. Robbiola, J.M. Blengino, C. Fiaud, Morphology and mechanisms of formation of natural patinas on archaeological CuSn alloys, Corros. Sci. 40 (1998) 2083–2111.

[6] I. Constantinides, A. Adriaens, F. Adams, Surface characterization of artificial corrosion layers on copper alloy reference materials, Appl. Surf. Sci. 189 (2002) 90–101.

[7] S. Neodo, D. Carugo, J.A. Warthon, K.R. Stokes, Electrochemical behaviour of nickel-aluminium bronze in chloride media: Influence of pH and benzotriazole, J. Electroanal. Chem. 695 (2013) 38–46.

[8] A. Romeiro, C. Gouveia-Caridade, C.M.A. Brett, Polyhenazine films as inhibitors of copper corrosion, J. Electroanal. Chem. 688 (2013) 282–288.

[9] K. Krishnaveni, J. Ravichandran, Influence of aqueous extract of leaves of Morinda tinctoria on copper corrosion in HCl medium, J. Electroanal. Chem. 735 (2014) 24–31.

[10] C. Rahal, M. Masmoudi, R. Abdelhedi, R. Sabot, M. Jeannin, M. Bouaziz, P. Refait, Olive leaf extract as natural corrosion inhibitor for pure copper in 0.5 M NaCl solution. A study of voltammetry around OCP, J. Electroanal. Chem. 769 (2016) 53–61.

[11] L. Robbiola, R. Portier, A global approach to the authentication of ancient bronzes based on the characterization of the alloy–patina–environment system, J. Cult. Herit. 7 (2006) 1–12.

[12] C. Chiavari, K. Rahmouni, H. Takenouti, S. Joiret, P. Vermaut, L. Robbiola, Composition and electrochemical properties of natural patinas of outdoor bronze monuments, Electrochim. Acta 52 (2007) 7760–7769.

[13] M.C. Bernard, S. Joiret, Understanding corrosion of ancient metals for the conservation of cultural heritage, Electrochim. Acta 54 (2009) 5199–5205.

[14] V. Costa, K. Leyssens, A. Adriaens, N. Richard, F. Scholz, Electrochemistry reveals archaeological materials. J. Solid State Electrochem. 14 (2010) 449–451.

[15] M.F. Alberghina, R. Barraco, M. Brai, T. Schillaci, L. Tranchina, Integrated analytical methodologies for the study of corrosion processes in archaeological bronzes. Spectrochim. Acta B 66 (2011) 129–137.

[16] M. Griesser, W. Kockelmann, K. Hradil, R. Traum, New insights into the manufacturing technique and corrosion of high leaded antique bronze coins, Microchem. J. 126 (2016) 181–193.

[17] A. Inberg, D. Ashkenazi, M. Cohen, N. Iddan, D. Cvikel, Corrosion products and microstructure of copper alloy coins from the Byzantine-period Ma'agan Mikhael B shipwreck, Israel. Microchem. J. 143 (2018) 400–409.

[18] M. Crosera, E. Baracchini, E. Prenesti, A. Giacomello, B. Callegher, P. Oliveri, G. Adami, Elemental characterization of surface and bulk of copper-based coins from the byzantine-period by means of spectroscopic techniques, Microchem. J. 147 (2019) 422–428.

[19] F. Scholz, B. Meyer, Voltammetry of solid microparticles immobilized on electrode surfaces, in Electroanalytical Chemistry, A Series of Advances. A.J. Bard, I. Rubinstein, Eds., Marcel Dekker, New York, vol. 20, pp 1–86, 1998.

[20] F. Scholz, U. Schröder, R. Gulabowski, A. Doménech-Carbó, Electrochemistry of Immobilized Particles and Droplets, 2nd ed. Springer, Berlin-Heidelberg.

[21] A. Doménech-Carbó, J. Labuda, F. Scholz, Electroanalytical chemistry for the analysis of solids: characterization and classification (IUPAC Technical Report), Pure Appl. Chem. 85 (2013) 609–631.

[22] A. Doménech-Carbó, M.T. Doménech-Carbó, V. Costa, Electrochemical Methods in Archaeometry, Conservation and Restoration (Monographs in Electrochemistry series, Scholz F, Ed.). Springer, Berlin-Heidelberg, 2009.

[23] A. Doménech-Carbó, Voltammetric methods applied to identification, speciation, and quantification of analytes from works of art: an overview, J. Solid State Electrochem. 14 (2010) 363–379.

[24] A. Doménech-Carbó, M.T. Doménech-Carbó, Electroanalytical techniques in archaeological and art conservation, Pure Appl. Chem. 90 (2018) 447–462.

[25] A. Doménech-Carbó, M.T. Doménech-Carbó, E. Montagna, C. Álvarez-Romero, Y. Lee, Electrochemical discrimination of mints: the last Chinese emperors Kuang Hsü and Hsüan T'ung monetary unification, Talanta 169 (2017) 50–56.

[26] F. Di Turo, N. Montoya, J. Piquero-Cilla, C. De Vito, F. Coletti, G. Favero, A. Doménech-Carbó, Archaeometric analysis of Roman bronze coins from the *Magna Mater* temple using solid-state voltammetry and electrochemical impedance spectroscopy, Anal. Chim. Acta 955 (2017) 36–47.

[27] A. Doménech-Carbó, M.T. Doménech-Carbó, C. Álvarez-Romero, N. Montoya, T. Pasíes-Oviedo, M. Buendía-Ortuño, Electrochemical characterization of coinage techniques the 17th century: The *maravedís* case, Electroanalysis 29 (2017) 2008–2018.

[28] M.T. Doménech-Carbó, C. Álvarez-Romero, A. Doménech-Carbó, L. Osete-Cortina, M.L.

Martínez-Bazán, Microchemical surface analysis of historic copper-based coins by the combined use of FIB-FESEM-EDX, OM, FTIR spectroscopy and solid-state electrochemical techniques. Microchem. J. 148 (2019) 573–581.

[29] A. Doménech-Carbó, M.T. Doménech-Carbó, C. Álvarez-Romero, T. Pasíes-Oviedo, M. Buendía-Ortuño, Screening of Iberian coinage in the 2th-1th BCE period using the voltammetry of immobilized particles, Electroanalysis 31 (2019) 1164–1173.

[30] A. Doménech-Carbó, M. Donnici, C. Álvarez-Romero, S. Daniele, M.T. Doménech-Carbó, (2021) Multiple-scan voltammetry of immobilized particles of ancient copper/bronze coins, J. Solid State Electrochem. 25 (2021) 195–206.

[31] A. Doménech-Carbó, B. Ramírez-Barat, C. Petiti, S. Goidanich, M.T. Doménech-Carbó, E. Cano, Characterization of traditional artificial patinas on copper using the voltammetry of immobilized particles, J. Electroanal. Chem. 877 (2020) artic. 114494.

[32] A. Doménech-Carbó, M.T. Doménech-Carbó, S. Capelo, T. Pasíes-Oviedo, I. Martínez-Lázaro, Dating archaeological copper/bronze artifacts using the voltammetry of microparticles, Angew. Chem. Int. Ed. 53 (2014) 9262–9266.

[33] A. Doménech-Carbó, M.A. Peiró-Ronda, J. Vives-Ferrándiz, G.S. Duffó, S. Farina, 'Dry' electrochemistry: a non-invasive approach to characterize archaeological iron objects, Electrochm. Commun. 125 (2021) artic. 106992.

[34] A. Sassolini, N. Colozza, E. Papa, K. Hermansson, I. Cacciotti, F. Arduini, Screen-printed electrode as a cost-effective and miniturized analytical tool for corrosion monitoring of reinforced concrete, Electrochem. Commun. 98 (2019) 69–72.

[35] G.S. Duffó, S.B. Farina, C.M. Giordano, Characterization of solid embeddable reference electrodes for corrosion monitoring in reinforced concrete structures, Electrochim. Acta 54 (2009) 1010–1020.

[36] A.S.T.M. Standard, C876: Standard Test Method for Corrosion Potentials of Uncoated Reinforcing Steel in Concrete, ASTM International, West Conshohocken, PA, 2009.

[37] M. Mödlinger, Herstellung und Verwendung bronzezeitlicher Schwerter Mitteleuropas. Eine vertiefende Studie zur mittelbronze- und urnenfelderzeitlichen Bewaffnung und Sozialstruktur. Universitätsforschungen zur prähistorischen Archäologie, 2011.

[38] M. Mödlinger, Protecting the body in war and combat: metal body armour in Bronze Age Europe, Oriental and European Archaeology 6, Wien: ÖAW, 2017.

[39] M. Mödlinger, P. Piccardo, Manufacture of Eastern European decorative discs from 1200 BC, J. Archaeol. Anthropol. Sci. 5/4 (2013) 299–309.

[40] M. Mödlinger, Z. El Morr, European Bronze Age sheet metal objects: 3000 years of high-level bronze manufacture. JOM 66/1 (2014) 171–177.

[41] M. Mödlinger, M. Pfisterer, Kontermarken und Abschrotspuren: Metallographische Analyse zweier römischer Gussmünzen, Mitteilungen der Österr. Numismatischen Gesellschaft 45/1 (2005) 16-23.

[42] A. Doménech-Carbó, M. Donnici, C. Álvarez-Romero, S. Daniele, M.T. Doménech-Carbó, Multiple-scan voltammetry of immobilized particles of ancient copper/bronze coins. J. Solid State Electrochem. 25 (2021) 195–206.

[43] V. Bongiorno, S. Campodonico, R. Caffara, P. Piccardo, M.M. Carnasciali, Micro- Raman spectroscopy for the characterization of artistic patinas produced on copper- based alloys, J. Raman Spectrosc. 43 (2012) 16-17.

[44] E. Basso C. Invernizzi, M. Malagodi, M.F. La Russa, D. Versan, P.P. Lottici, Characterization of colorants and opacifiers in roman glass mosaic tesserae through spectroscopic and spectrometric techniques, J. Raman Spectrosc. 45 (2014) 238–245.

[45] N. Montoya, E. Montagna, M.T. Doménech-Carbó, A. Doménech-Carbó, Raman spectroscopy characterization of ten-cash productions from the late Chinese emperors to the republic, J. Raman Spectrosc. 48 (2017) 1337–1345.

[46] D. Neff, P. Dillmann, M. Descostes, G. Beranger, Corrosion of iron archaeological artefacts in soil: Estimation of the average corrosion rates involving analytical techniques and thermodynamic calculations, Corros. Sci. 48 (2006) 2947–2970.

[47] M.S. Venkatraman, I.S. Cole, B. Emmanuel, Model for corrosion of metals covered with thin electrolyte layers: Pseudo-steady state diffusion of oxygen, Corros. Sci. 56 (2011) 7171–7179.

[48] M.S. Venkatraman, I.S. Cole, B. Emmanuel, Corrosion under a porous layer: A porous electrode model and its implications for self-repair, Corros. Sci. 56 (2011) 8192–8203.

Tables

Table 1. Objects studied. All objects were initially cast (c) and, in most cases, underwent different amounts and numerous cycles of cold deformation and annealing (d/a). The final working step was either annealing (af) or cold deformation (df). One of the coins was hallmarked after casting (no. 20). For the chemical composition, mayor elements are indicated. Usually, small amounts (<0.5 wt.%) of As, Sb, S, and Fe are also present.

no.	museum	inv.no.	Object	Type	find spot	state	context	chronology	thermo-mechanical history	Cu
1	Wels	10.924	sword	Erlach	Unterschauersberg	Austria	water	HaA	c; a/d, df	87.2
2	Vöcklabruck	I 14	sword	Erlach	Desselbrunn/Rüsdorf	Austria	water	HaA	c; a/d, df	86
3	Linz	4624	sword	Rixheim	Linz	Austria	water	BzD	c; a/d, af	Cu
4	Wels	12.697	sword	Reutlingen	Wels-Waidhausen	Austria	water	D – HaA1	c; a/d, df	89.6
5	Institut UFG	26.440	sword	early type	Au am Leithagebirge	Austria	grave	BzB1	c; a/d, df	85.7
6	Melk	546	sword	Unterradl	Unterradl	Austria	grave	HaA(1)	c; a/d, df	89.1
7	NHM Wien	12.638	sword	Aldrans	Tscheraditz	Czech Republic	grave	HaA2	c; df	91
8	NHM Wien	1926	sword	Wörschach	Vulchovica	Ukraine	hoard	HaB1	c; df	91.2
9	Livno	none	helmet	early Iron Age	Grepci	Bosnia-Herzegov.	grave	HaB2/C1	c; a/d, df	88.0
10	NHM Wien	47.626	helmet	crested	Škocjan	Slovenia	deposit	HaB	c; a/d, df	89.8
11	NHM Wien	47.633	helmet	crested	Škocjan	Slovenia	deposit	HaB	c; a/d, df	88.2
12	Zemaljski	A-1805	helmet	Paks	Poljanci I	Croatia	hoard	BzD/HaA1	c; a/d, df	87.1
13	Brukhental	11.992	helmet	Pişcolt	Şoarş	Romania	hoard	HaB1	c; a/d, df	87.3
14	Zagreb	10.237	helmet	Paks	Veliko Nabrđe	Croatia	hoard	BzD/HaA1	c; a/d, df	87.9
15	Croatia	shield 1	shield	shield 1	Otok Privlaka	Croatia	hoard	HaA/B	c; a/d, df	92.3
16	Croatia	shield 2	shield	shield 2	Otok Privlaka	Croatia	hoard	HaA/B	c; a/d, df	90.7
17	Zemaljski	A-4026	applique	applique	Poljanci IV	Croatia	hoard	BzD/HaA1	c; a/d, df	90.6
18	Zemaljski	3730, 3734	helmet	Paks (cheek plate)	Podcrkavlje-Sl. Brod	Croatia	hoard	BzD/HaA1	c; a/d, df	87.3
19	none	none	coin*	Sesterz Antoninus III	none	Austria	hoard	211-217 AD	c	no a
20	none	none	coin**	TI.C.A Kontermarke	none	Austria	hoard	2nd/3rd c. AD	c	no a

Table 2. Statistical parameters corresponding to the fit of experimental $Q_p(N)$ vs. $1/N$ data to 2nd order polynomial functions and values of the $Q_p(2)/Q_p(6)$ and $Q_p(2)/Q_p(\text{lim})$ ratios. From SWVs performed at graphite electrodes modified with samples **2** and **3** immersed into 0.25 M HAc/NaAc aqueous solution at pH 4.75 in conditions such as in Figure 1.

Sample	Equation	r	$Q_p(2)/Q_p(6)$	$Q_p(2)/Q_p(\text{lim})$
2	$Q_p(N) = 7.3(1/N)^2 - 17.4(1/N) + 14.8$	0.9998	0.658	0.540
2	$Q_p(N) = 7.8(1/N)^2 - 17.0(1/N) + 13.8$	0.9998	0.574	0.449
2	$Q_p(N) = 3.1(1/N)^2 - 5.9(1/N) + 3.9$	0.998	0.652	0.529
3	$Q_p(N) = 44.0(1/N)^2 - 79.6(1/N) + 44.2$	0.9994	0.443	0.321
3	$Q_p(N) = 21.7(1/N)^2 - 41.7(1/N) + 25.6$	0.9994	0.536	0.406
3	$Q_p(N) = 17.2(1/N)^2 - 30.6(1/N) + 15.9$	0.998	0.449	0.357

Figures

Figure 1. a) Fragments from a Late Bronze Age helmet Type Paks, found in Veliko Nabrđe, Croatia. On the left, the metallographic cross-section with a detail of the corrosion structure in polarized light (centre). On the right, a complete helmet of the same type. b) Bronze Age sword no. 8, found in Viljĥovicja (Vulchovica), Ukraine. The location of the metallographic sample is indicated with an arrow. Below the arrow, the cross-section of the corrosion in polarized light is visible. Above it, the etched microstructure of the central area of the blade (etchant: Klemm II) and the edge of the blade (etchant: ammonium persulfate). c) Late Bronze Age / Early Iron Age helmet knob, found in Grepci, Bosnia-Herzegovina (no. 9). The location of the metallographic sample is indicated with an arrow. Note the SEM-image of the corrosion structure (metal core is below; dark-grey CuS-inclusions are visible).

Figure 2. Schematics of the OCP measurements performed in this study on epoxy resin-embedded cross-sections of archaeological objects.

Figure 3. Multiple-(1st to 6th)-scan SWVs of samples a) **2**, b) **4**, c) **7** and d) **10** attached to graphite electrode in contact with 0.25 M HAc/NaAc aqueous solution at pH 4.75. Potential scan initiated at a) 0.45 V in the negative direction; potential step increment 4 mV; square wave amplitude 25 mV; frequency 10 Hz. The dotted line represents the base line used for peak current measurement in the 1st scan.

Figure 4. Variation with the scan number N of: a) the peak current $I_p(N)$ of the signal C_1 (taken from series of SWVs such as in Figure 3), and b) the accumulated peak current $Q_p(N)$ measured after sampling in three different spots of sample **3**. The continuous lines correspond to the fit of experimental points to a potential function taken N as a continuous variable.

Figure 5. Representation of $Q_p(N)$ vs. $1/N$ from three replicate voltammetric measurements in different spots of sample **3** in conditions such as in Figure 3. The continuous lines correspond to the fit of experimental points to a 2nd order polynomial function taken N as a continuous variable in order to extrapolate the value of $Q_p(lim)$.

Figure 6. Schematic representation of the variation of $Q_p(N)$ with depth for two different bronze patinas in repetitive scan voltammetric measurements. For simplicity, a linear variation was taken and it is assumed that the successive scans similarly delaminate both patinas.

Figure 7. a) Experimental OCP vs. time curves recorded for samples **4** and **8**. b) Plots of $\ln(V_{OCP}-V_{lim})$ vs. time for samples **2**, **3**, and **11** (error bars omitted for clarity). c) Equivalent circuit used to model V_{OCP} vs. t measurements.

Figure 8. Plots of $Q_p(2)/Q_p(lim)$ vs. age for samples: a) **1**-**8**, b) **9**-**20**, all submitted to cast, annealing and cold deformation. The continuous line corresponds to the fit of the data to a potential function.

Figure 9. Plots of V_{lim} vs. age for samples **1**-**8** from OCP measurements such as in Figure 7a. The continuous line corresponds to the fit of the data to a potential function. Error bars correspond to the extreme values recorded in three replicate measurements.
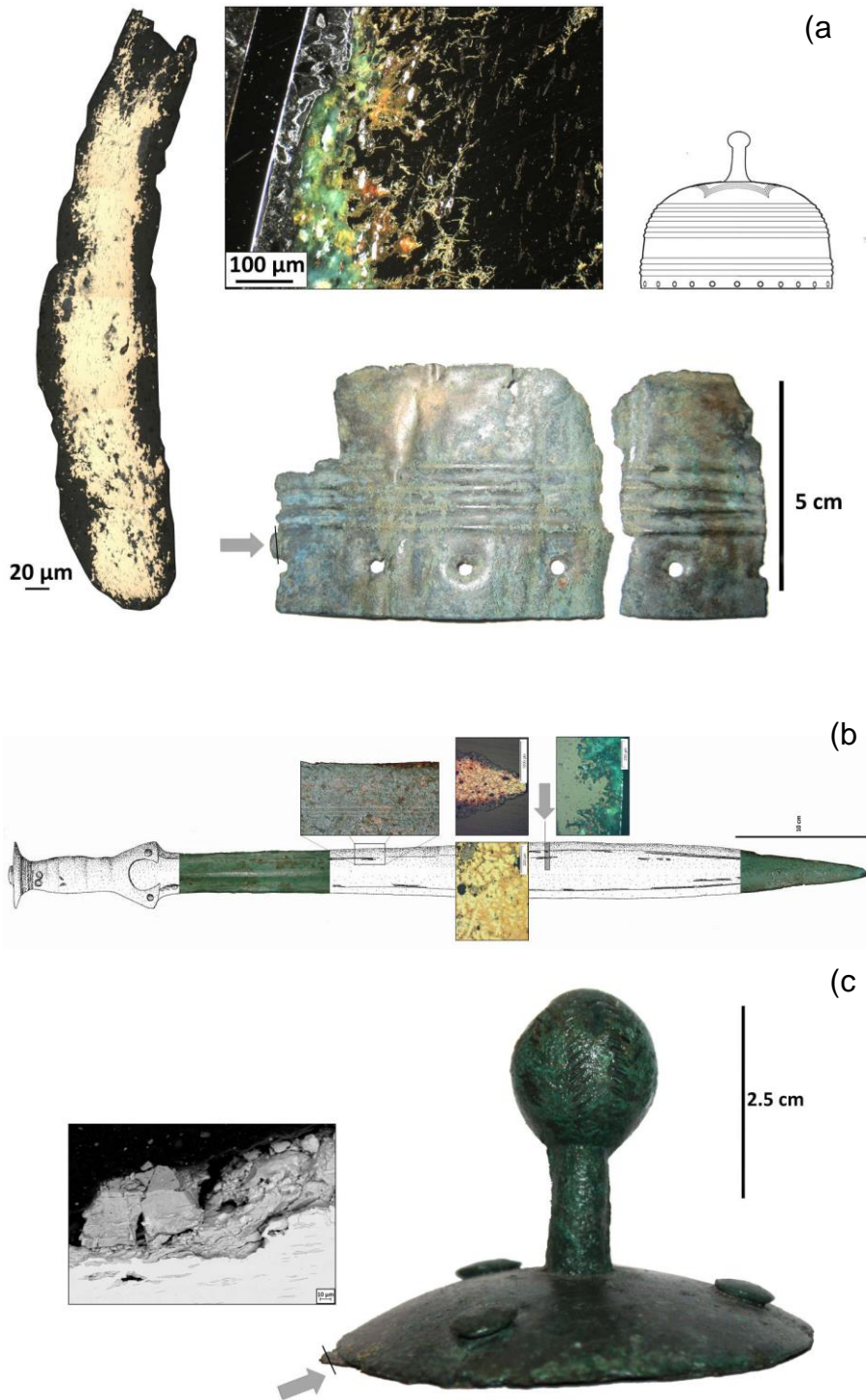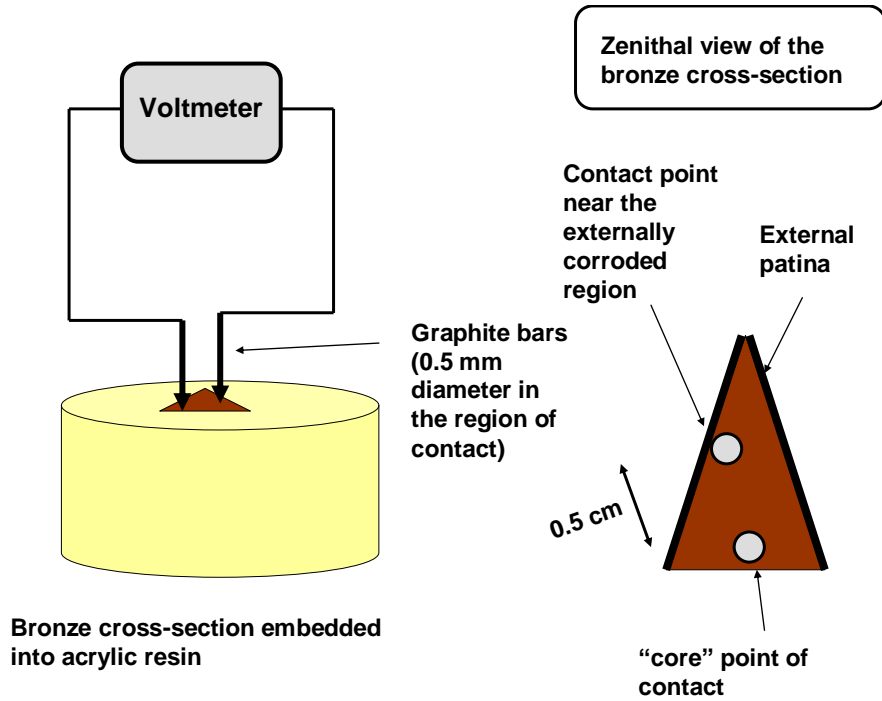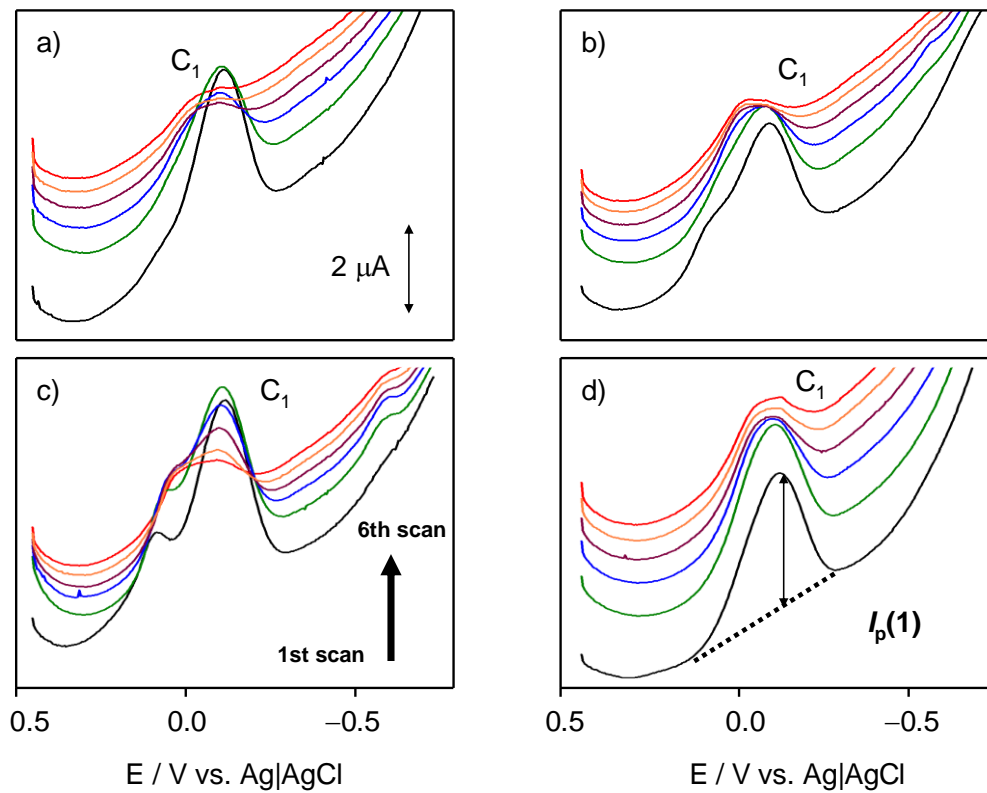
Figure 1.

(a

(b

(c

Figure 2.

Voltmeter

Graphite bars
(0.5 mm
diameter in
the region of
contact)

Bronze cross-section embedded
into acrylic resin

Zenithal view of the
bronze cross-section

Contact point
near the
externally
corroded
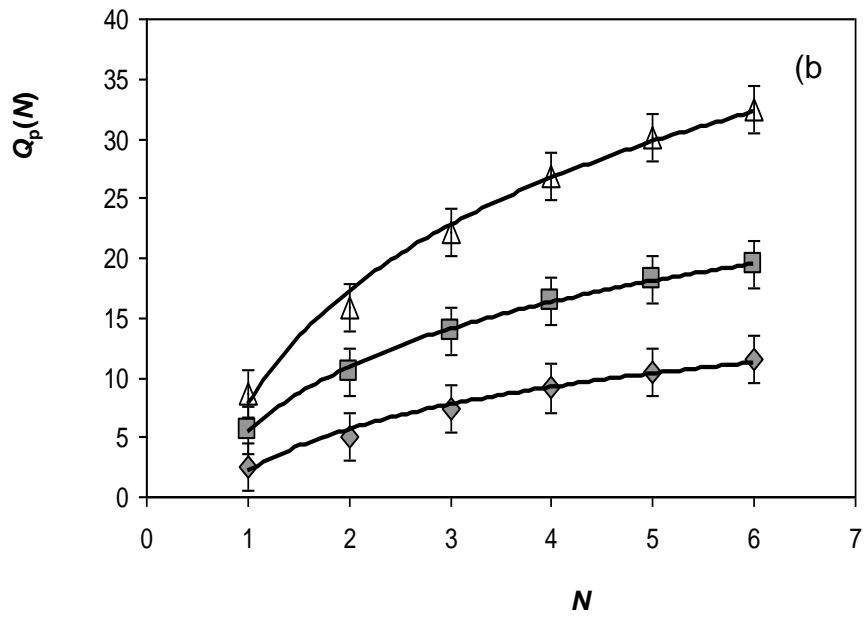region

External
patina

0.5 cm

"core" point of
contact
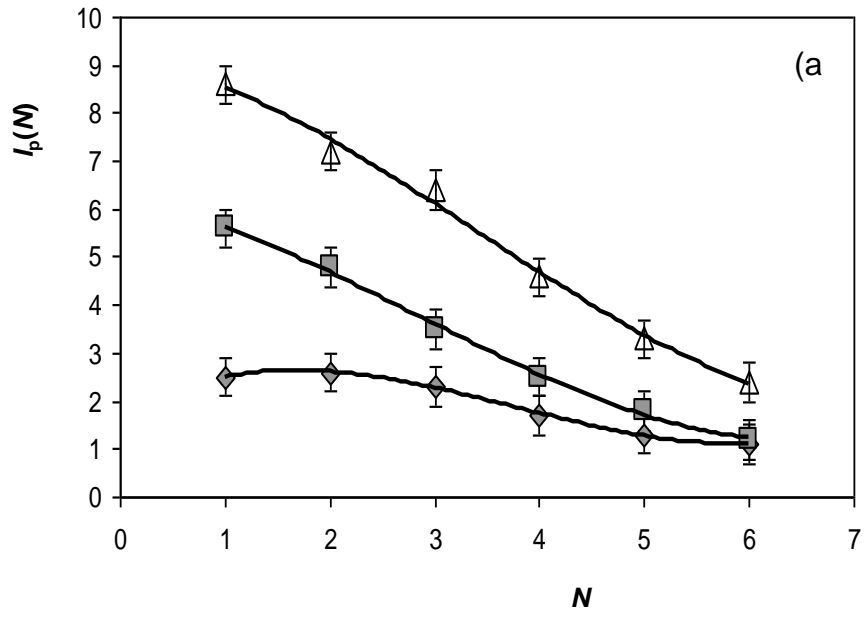
Figure 3.
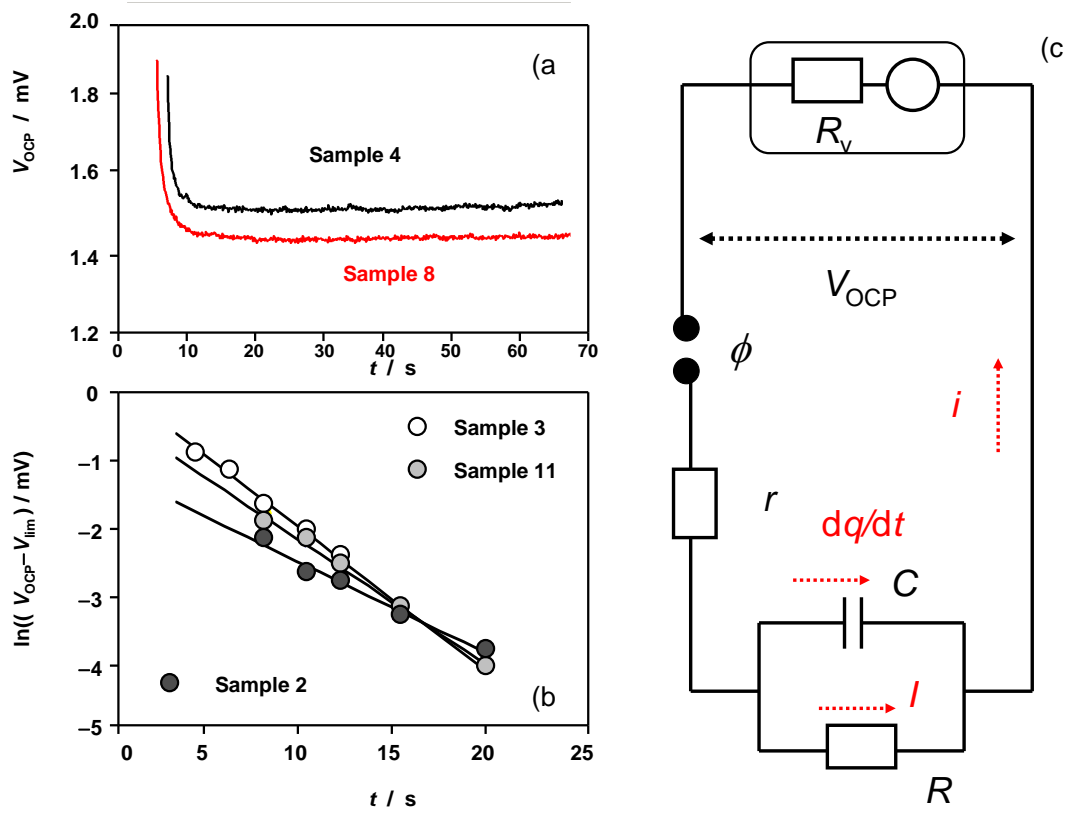
Figure 4.

Figure 5.
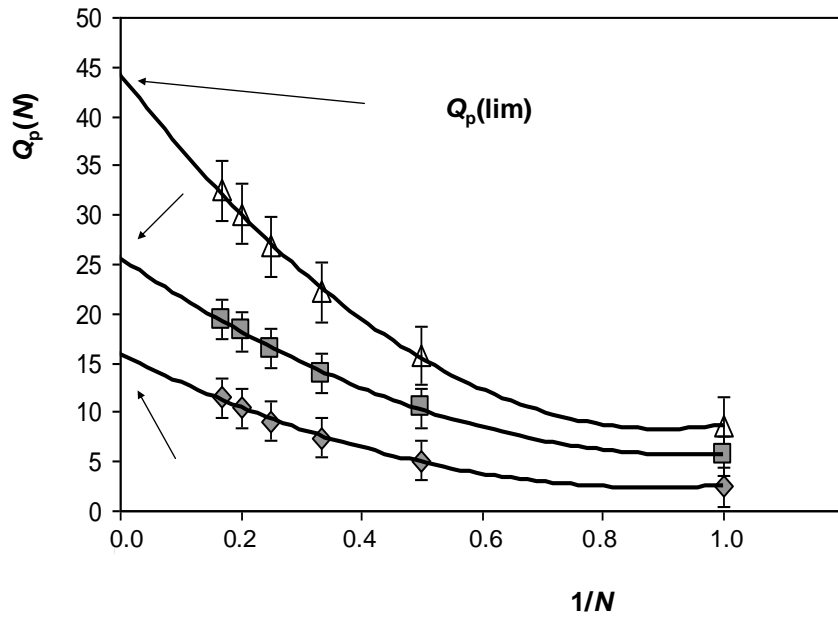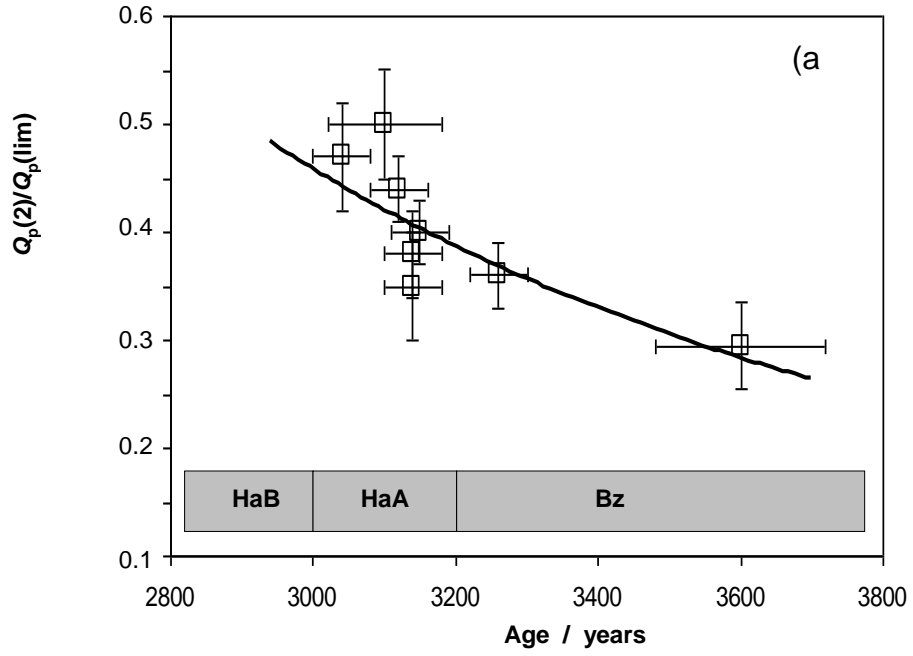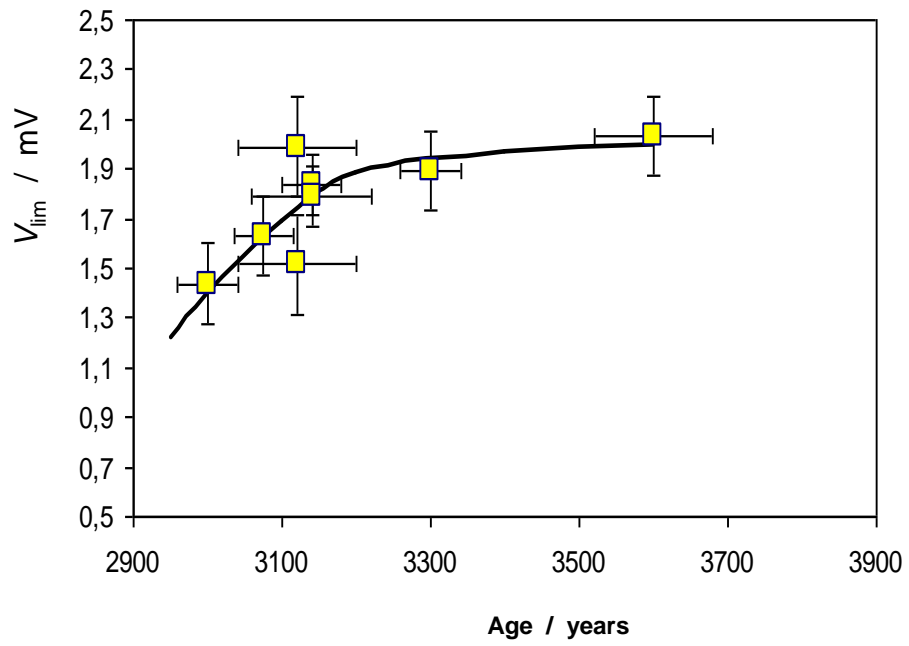
Figure 6.
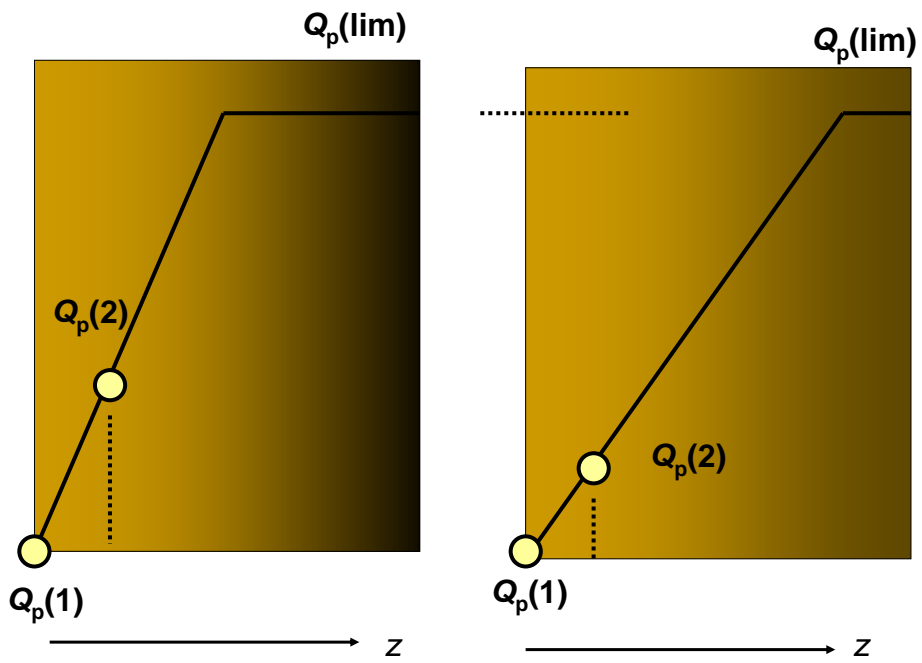
Figure 7.

Figure 8.
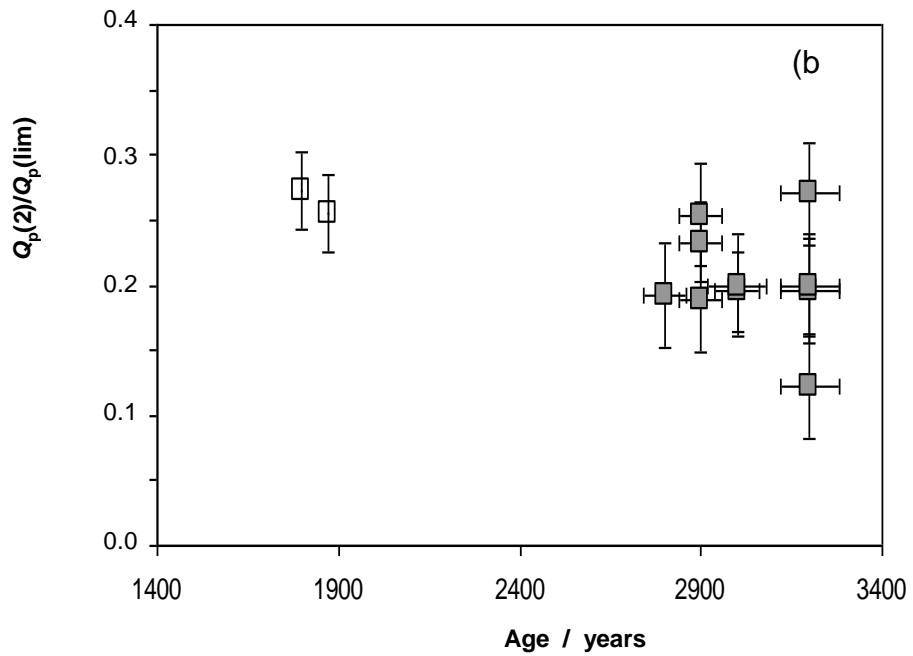
Figure 9.

Authors' contribution:

ADC conceived the research, performed electrochemical measurements, developed the theoretical model and wrote the manuscript; MM provided archaeological information, discussed the results and contributed to planning and writing the manuscript; TDC contributed to planning and writing of the manuscript.

The authors declare no competing interest.